Faraday Discussions

Cite this: *Faraday Discuss.*, 2018, **208**, 255

PAPER

In situ formation of the active sites in Pd–Au bimetallic nanocatalysts for CO oxidation: NAP (near ambient pressure) XPS and MS study

A. V. Bukhtiyarov, [a] I. P. Prosvirin, [ab] A. A. Saraev, [ab] A. Yu. Klyushin, [c] A. Knop-Gericke[c] and V. I. Bukhtiyarov *[ab]

Received 19th December 2017, Accepted 24th January 2018
DOI: 10.1039/c7fd00219j

Model bimetallic Pd–Au/HOPG catalysts have been investigated in the CO oxidation reaction using a combination of NAP XPS and MS techniques. The samples have shown catalytic activity at temperatures above 150 °C. The redistribution of Au and Pd on the surface depending on the reaction conditions has been demonstrated using NAP XPS. The Pd enrichment of the bimetallic particles' surface under reaction gas mixture has been shown. Apparently, CO adsorption induces Pd segregation on the surface. Heating the sample under reaction conditions above 150 °C decomposes the Pd–CO state due to CO desorption and reaction and simultaneous Pd–Au alloy formation on the surface takes place. Cooling back down to RT results in reversible Pd segregation due to Pd–CO formation and the sample becomes inactive. It has been shown that *in situ* studies are necessary for investigation of the active sites in Pd–Au bimetallic systems.

1. Introduction

The ability of a second metal to improve the catalytic performance of supported monometallic particles has led to great interest in bimetallic catalysts.[1–5] Dilution of the metal particle surface with the second metal allows the formation of active sites with a specific geometry (ensemble effect) and/or modification of the electronic property of an active metal (ligand effect). As a consequence, catalytic activity of the bimetallic catalyst can become much higher than the activities of monometallic ones – the synergistic effect appears in this case. However, despite a large number of investigations of various bimetallic catalysts published in the last decade, the reasons for the synergistic effects observed for the specific catalytic systems are still under discussion in many cases.

[a]*Boreskov Institute of Catalysis, SB RAS, Lavrentieva Ave. 5, Novosibirsk, 630090, Russia. E-mail: vib@catalysis.ru*
[b]*Novosibirsk State University, Pirogova Str. 2, Novosibirsk, 630090, Russia*
[c]*Fritz-Haber-Institute der Max Planck Society, Faradayweg 4-6, Berlin, 14195, Germany*

One of the most evident explanations of such uncertainties, which has been supported by many researchers, is the flexibility of the surface composition of bimetallic particles.[1–3,6–12] Indeed, not only the ratio of the introduced metals, but also the temperature of calcination and influence of the reaction mixture will change the surface composition. A remarkable example of the dynamical restructuring at the nanoscale was reported in a recent *in situ* TEM and XPS study of methanol oxidation over gold–silver alloy catalysts.[13] The authors demonstrated a direct dependence of oxidation activity on the changing surface silver concentration under the influence of reaction conditions.

The Pd–Au bimetallic systems used as catalysts for a number of reactions, such as vinyl acetate synthesis,[6] low temperature CO oxidation,[7,8] NO reduction,[9] direct formation of hydrogen peroxide from $H_2 + O_2$ mixture,[10] *etc.*, are also not free from this uncertainty. Even for such a simple reaction as CO oxidation, the catalytic results are controversial. An enhancement of catalytic activity in low-temperature CO oxidation was observed for the Au/SnO_2 and Au/TiO_2 systems after their doping with Pd.[14,15] On the other hand, all $Pd–Au/SiO_2$ catalysts were catalytically less active than Au/SiO_2.[7] A similar result was reported for the $Pd–Au/Al_2O_3$ catalysts.[15] These data seem to indicate the influence of the support on the catalytic properties of bimetallic catalysts.

At the same time, some extremely controversial results on dependencies of catalytic activity in CO oxidation on the Pd/Au ratio were reported in two papers from different authors for similar samples – Pd–Au particles supported on silica, which is the most inert support. Indeed, if the catalysts with enhanced Au loading ($Pd/Au \leq 1$) exhibit lower activity than pure palladium in both papers,[7,16] then increasing the Pd content above $Pd/Au > 1$ either improves considerably the catalytic activity[7] or does not change it.[16] One more paper reported higher low-temperature activity ($T < 100$ °C) of the $Pd–Au/SiO_2$ catalysts compared with a monometallic Pd/SiO_2 sample; the latter becomes more active than bimetallic ones at higher temperatures ($T > 120$ °C).[17] Again, the reported differences in catalytic data can be explained by variation of the surface composition of Pd–Au particles under the influence of the reaction conditions. This proposal is based on the well-known fact that the surface of bimetallic Pd–Au particles can be enriched with gold at $T > 200$ °C (ref. 1) or with palladium in the presence of CO at $T \leq 150$ °C.[18,19] It is evident that to determine the exact surface composition of bimetallic particles in the presence of the reaction mixture *in situ* physical methods have to be applied. Understanding this aspect, the authors of the cited papers performed *in situ* investigations of bimetallic Pd–Au catalysts with environmental TEM, polarization modulation infrared absorption spectroscopy (PM IRAS), diffusion reflectance infrared Fourier transform spectroscopy (DRIFTS), near ambient pressure XPS (NAP XPS), *etc.*

In this paper, NAP XPS and mass spectrometry were used to study *in situ* the active site formation in bimetallic Pd–Au catalysts for CO oxidation. To reach the goal, two different Pd–Au/HOPG (highly oriented pyrolytic graphite) model bimetallic catalysts were prepared by a special procedure *via* sequential high-vacuum physical vapor deposition (PVD) of gold and then palladium, and characterized by XPS and scanning tunneling microscopy (STM) before and after *in situ* characterization (see Experimental section). Application of model samples is a very useful approach to reveal a correlation of electronic properties and

morphology of bimetallic particles produced under reaction conditions with their catalytic performance.[20–24]

2. Experimental

2.1. Pd–Au/HOPG catalyst preparation and characterization

Preparation of the samples and their primary characterization was done in a SPECS photoelectron spectrometer (Germany) equipped with hemispherical analyzer PHOIBOS-150-MCD-9, ellipsoidal monochromator FOCUS500, and X-ray source XR 50M with double Al/Ag anode.

Commercially available HOPG (7 × 7 mm, approximately 1 mm thickness, SPI supplies, Grade SPI-2) was used as a support for the bimetallic Pd–Au catalysts. Before loading into the spectrometer, each sample of HOPG was cleaned by removing the upper layers with Scotch tape. Then it was loaded into the SPECS spectrometer and annealed at 700 °C under ultra-high vacuum (UHV) conditions for 3 h to remove surface contaminations. Then the cleaned and annealed HOPG surface was etched smoothly with argon ions (t = 3–4 s, P(Ar) = 3 × 10^{-6} mbar and accelerating voltage of 0.5 kV) using an IQE 11/35 ion gun to create the surface defects serving as an anchor for the deposited gold particles. Deposition of gold on the defective HOPG surface was carried out in the preparation chamber of the SPECS spectrometer using an Omicron EFM3 electron beam evaporator. Before subsequent deposition of palladium, the Au/HOPG matrix was heated at 300 °C in UHV to anneal the defects and finally to stabilize the gold particles against sintering. We developed this procedure earlier and tested it on the Ag/HOPG samples.[20] The same procedure was applied for the preparation of the pure Pd/HOPG surface used as a blank sample in this work.

Two samples with alloyed bimetallic Pd–Au nanoparticles supported on HOPG surface with different Pd/Au ratios were prepared by PVD of Pd on the stabilized Au/HOPG matrixes followed by heating in UHV up to 400 °C in order to form Pd–Au alloyed particles.[25] In all stages of the preparation procedure the samples were investigated by XPS, using regular SPECS and synchrotron-based RGBL (Russian–German beam line) photoelectron spectrometers located in BIC (Novosibirsk, Russia) and in Helmholtz Centrum of Berlin (Germany).[25]

STM measurements of the prepared Pd–Au/HOPG samples (fresh, annealed, and RM-activated) were carried out using an UHV 7000 VT microscope (RHK Technology, USA) operating in constant current mode. The STM tips used in the experiments were cut Pt–Ir tips. The standard samples like Si (111) single crystal with 7 × 7 reconstruction and clean HOPG were used for scanner calibration.

2.2. NAP XPS experiments

In situ experiments were carried out with an NAP XPS system at the ISISS beam line at BESSY II/HZB (Berlin, Germany).[26] The Pd–Au/HOPG and Pd/HOPG samples were placed between a stainless steel backplate and a lid (with 6 mm hole) and mounted onto a sapphire sample holder. The samples were heated up from the back side using the infrared laser and the temperature was measured with a K-type thermocouple. The CO : O_2 = 2 : 1 mixture was introduced into the high-pressure cell up to 0.25 mbar by the mass-flow controllers (MFC). Before loading in CO + O_2 reaction mixture, all Pd–Au/HOPG samples were heated up to

300 °C under UHV in order to remove the contaminations from the surface. The experiments during the CO oxidation reaction were performed as follows: the CO + O_2 flow (CO : O_2 = 2 : 1; P = 0.25 mbar) was flowed into the gas cell at RT, then the samples were heated step by step up to 250 °C (RT–100–150–200–230–250 °C), while XPS and MS spectra were measured at each temperature. It should be noted that all XPS lines from gold, palladium and carbon (Au 4f, Pd 3d and C 1s) at each temperature were measured three times at different values of kinetic energy: 300, 450 and 600 eV, providing a variation of depth of electron emission. To estimate the depth of analysis for these different kinetic energies we used the average values of inelastic mean free paths (IMFP) of electrons in metallic gold and palladium −5.9, 7.6 and 9.2 Å, respectively.[27]

To determine the positions of the peaks in the Au 4f and Pd 3d spectra, XPS peaks were calibrated against the C 1s spectra (binding energies (BE) = 284.5 eV) taken at the same primary excitation energies as Au 4f and Pd 3d. Spectral analysis and data processing were performed with the XPS Peak 4.1 program.[28] For the quantitative analysis the integral intensities of the Au 4f, Pd 3d and C 1s lines were corrected using ionization cross-section data taken from Yeh and Lindau[29] and also were normalized with respect to current and photon flux. For the peak fitting of the Pd 3d signal, the Au $4d_{5/2}$ peak was subtracted from the spectra because of their overlapping. The shape and intensity of Au $4d_{5/2}$ were calculated from the less intensive Au $4d_{3/2}$ peak measured for the pure Au/HOPG sample.

3. Results and discussion

Table 1 shows atomic ratios for two bimetallic Pd–Au/HOPG samples calculated from XPS data taken at each step of the preparation procedure. The main difference in the samples was the amount of gold deposited during the initial step – Au/C atomic ratios were 0.024 and 0.009, whereas the amount of the Pd sequentially deposited was approximately the same (Pd/C ~ 0.1) for both samples. According to this, these samples will hereafter be called $PdAu_{high}$ and $PdAu_{low}$, respectively. Heating the initial monometallic Au/HOPG matrixes at 300 °C in UHV decreases slightly the Au/C atomic ratios (Table 1) due to formation and stabilization of 3D gold nanoparticles.[20] Final annealing of bimetallic Pd–Au/HOPG samples at 400 °C in UHV increases the Au/Pd atomic ratios compared with values measured directly after Pd deposition (Table 1) indicating the Pd–Au alloy formation.[25]

STM images of the prepared $PdAu_{high}$ and $PdAu_{low}$ catalysts are shown in Fig. 1. The $PdAu_{high}$ and $PdAu_{low}$ samples are characterized as 3D particles with a rather narrow particle size distribution at the mean particle sizes of 7.8 and

Table 1 Atomic ratios of elements calculated from XPS data (SPECS)

Sample	Au deposition Au/C	Heating in UHV Au/C	Pd deposition Pd/C	Annealing at 400 °C (alloy formation) Au/Pd	After *in situ* experiments Au/Pd
$PdAu_{high}$	0.024	0.019	0.011	1.61	2
$PdAu_{low}$	0.009	0.006	0.010	0.37	0.65

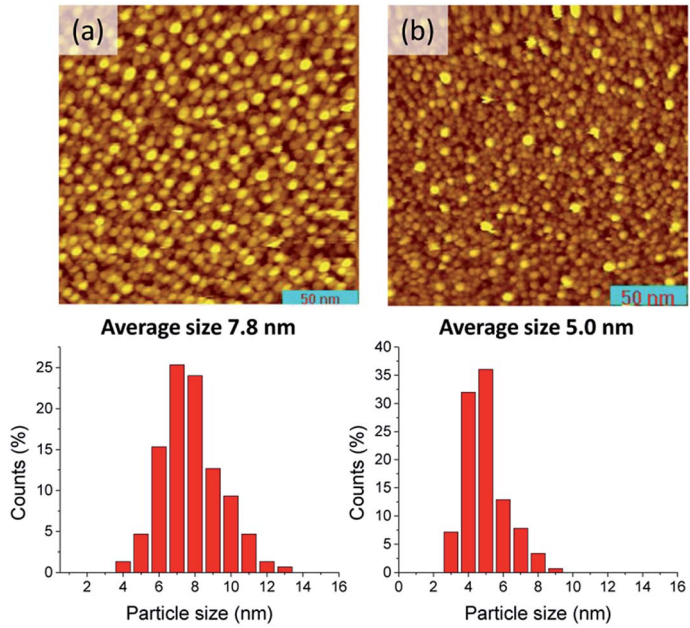

Fig. 1 STM images (200 × 200 nm) and the particle size distributions of Pd–Au/HOPG: (a) $PdAu_{high}$; (b) $PdAu_{low}$. Tunneling parameters: (a) 0.49 nA, −490 mV; (b) 0.52 nA, −1500 mV.

5.0 nm, respectively. The mean particle size ($\langle d \rangle$) was determined according to the equation:

$$\langle d \rangle = \frac{\sum_i (d_i \times N_i)}{\sum_i N_i},$$

where N_i is the number of particles with a diameter of d_i.

NAP XPS investigation of the alloyed Pd–Au/HOPG catalysts in CO oxidation ($CO : O_2 = 2 : 1$, $P = 0.25$ mbar) was performed using the ISISS station at the Berlin synchrotron radiation source BESSY II (HZB).[26] Fig. 2 shows CO_2 mass-spectrometric signal ($m/z = 44$), as well as the Au/Pd atomic ratios calculated from Au 4f and Pd 3d spectra, measured in the course of sample heating followed by cooling (from room temperature up to 250 °C and then down to RT). Although the Au 4f, Pd 3d and C 1s spectra for each temperature were measured three times with different excitation energies (see Experimental section), the Au/Pd ratios presented in this figure were calculated from the XPS spectra measured at a kinetic energy of 300 eV (surface location).

One can see that no catalytic activity is observed for bimetallic samples at $T \leq 150$ °C, whereas the intensity of CO_2 is increased at higher temperatures achieving the maximum at 250 °C. Reference experiments with pure HOPG did not show any catalytic activity towards the CO oxidation reaction under the same reaction conditions in the whole range of temperatures. Heating the sample also increases the Au/Pd atomic ratios for both samples (Fig. 2). Contrary to this observation, no

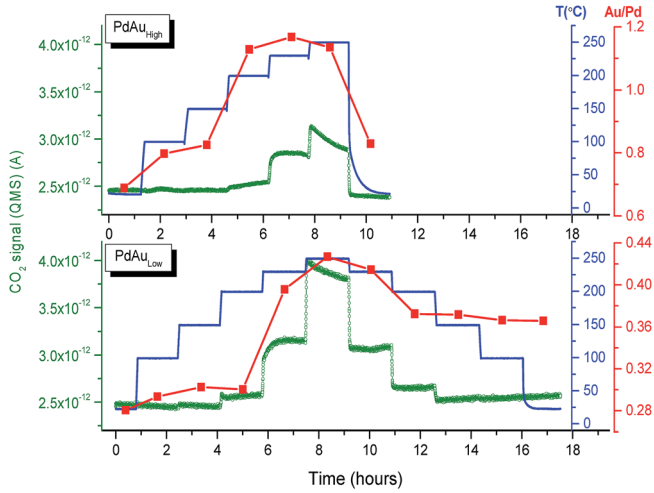

Fig. 2 CO_2 MS signal ($m/z = 44$) in the gas phase and Au/Pd atomic ratios calculated from Au 4f and Pd 3d spectra acquired from Pd–Au/HOPG samples in CO + O_2 gas mixture depending on temperature.

variation of the Au/Pd atomic ratio was observed in the reference experiments, when Pd–Au/HOPG samples were heated up to 300 °C in UHV. It should be noted that the heating in UHV up to 200 °C did not change the Au/Pd atomic ratio.[25] All these data indicate a transformation of the surface composition/structure of bimetallic particles under the influence of reaction mixture. Cooling the sample leads to a decrease in the Au/Pd atomic ratio indicating the reversible character of this transformation. Furthermore, these results suggest that variation of bimetallic particle sizes is hardly the reason for the observed variations of the Au/Pd atomic ratio.

STM data measured for the Pd–Au/HOPG catalysts before and after NAP XPS experiments prove this suggestion. Indeed, Fig. 3 shows that for the $PdAu_{low}$

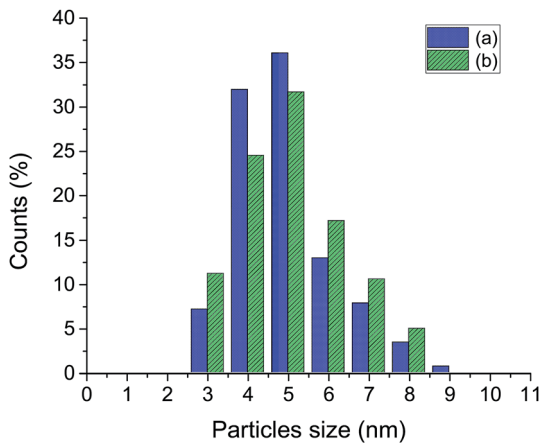

Fig. 3 Particle size distributions in $PdAu_{low}$ sample: (a) freshly prepared; (b) after NAP XPS experiments. The mean particle size is (a) 5.0 nm; (b) 5.1 nm.

catalyst both the particle size distributions and the mean particle size remained almost the same – compare the mean particle size of 5.1 nm for the treated catalysts with 5.0 nm for the fresh sample. This, together with the XPS data, which show similarity in the Au/Pd atomic ratio values for the freshly prepared and treated samples (Table 1, last two columns), leads us to a conclusion about the stability of the prepared bimetallic Pd–Au particles as a whole under reaction conditions. Then we can suggest that most of the changes in the XPS spectra are due to a redistribution of metals inside the bimetallic particles. Reversible variation in the Pd/Au atomic ratio during the heating–cooling cycle also indicates that the active state of the catalysts is produced only under reaction conditions ($T > 150\ ^{\circ}C$). As a consequence, only the application of *in situ* techniques is necessary to provide progress in understanding the state of the active surface in Pd–Au particles.

Fig. 4 shows the Au 4f spectra (left), as well as Au $4f_{7/2}$ binding energies and Au/C atomic ratios (right), for the $PdAu_{low}$ sample measured *in situ* in reaction mixture ($CO : O_2 = 2 : 1$, $P = 0.25$ mbar) at various temperatures. One can see the shift of the Au $4f_{7/2}$ peak position to lower binding energy together with the Au/C atomic ratio increasing with rising temperature. Back cooling of the sample changes the spectral characteristics reversibly. The shift to lower binding energies is an indicator of the alloy formation,[1,17,30] whereas the heating-induced increase in the Au/Pd atomic ratio points to surface segregation of gold and/or Pd diffusion into the bulk of the bimetallic particles under reaction conditions.[25]

A much more complex picture is observed for the Pd 3d region, which was corrected by subtracting the Au $4d_{5/2}$ signal from the experimentally measured spectra (see Experimental section). Fig. 5 shows the corresponding Pd $3d_{5/2}$ spectra with their deconvolution on several components depending on the sample temperature. Deconvolution of the original spectra was based on literature data where different Pd species were identified under different conditions.[1,7,25,30–36]

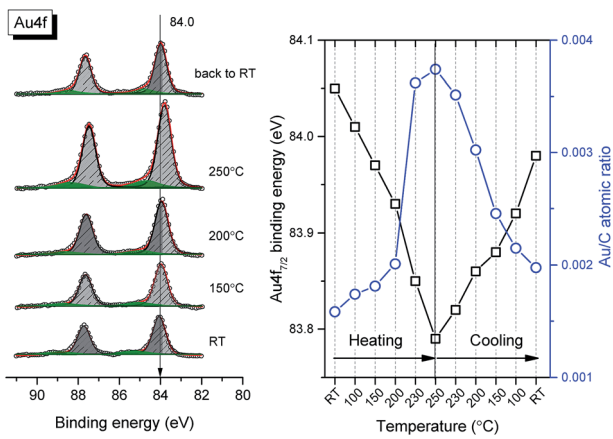

Fig. 4 Au 4f spectra (left) and variation of Au $4f_{7/2}$ binding energy and Au/C atomic ratio (right) with temperature taken for $PdAu_{low}$ sample under the reaction mixture (spectra were measured at 300 eV kinetic energy).

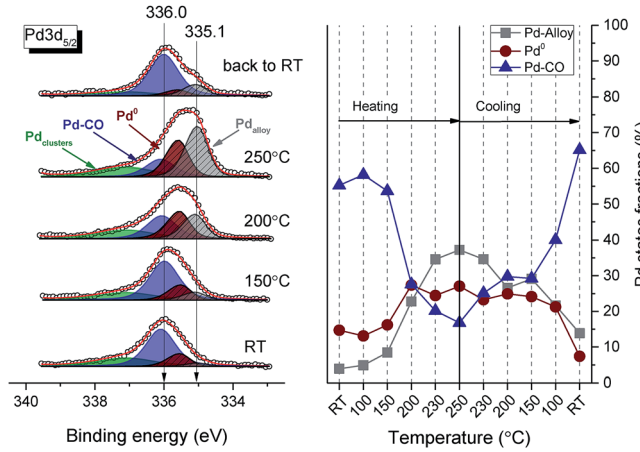

Fig. 5 Pd $3d_{5/2}$ spectra (left) and fraction of different Pd states (right) depending on the temperature taken for $PdAu_{low}$ sample under the reaction mixture (spectra measured at 300 eV kinetic energy).

For example, the Pd $3d_{5/2}$ peaks at binding energies (BE) of ~335.0 eV and ~335.6 eV were attributed to Pd in AuPd alloy[1,7,25,30] and metallic Pd,[1,30–32], respectively. There are also some papers[34–36] where the Pd $3d_{5/2}$ species with BE of about 336 eV was attributed to the CO-induced components of palladium due to adsorption of CO on bridge or on-top Pd sites. Moreover, Strømsheim *et al.*[35] used a combination of NAP XPS and QMS for investigation of CO oxidation over $Pd_3Au(100)$ single crystal to show the presence of two different Pd states with similar Pd $3d_{5/2}$ binding energy values (the difference was only 0.2 eV) corresponding to $Pd–CO_{ads}$ species and to oxidized Pd–O species. Finally, our recent papers[25,37] identified the Pd $3d_{5/2}$ peak at 337.2 eV as small Pd clusters attached to some defective sites on the HOPG surface.[33] It should be mentioned that all the spectral parameters (BE, FWHM, G/L ratio) for XPS peak fitting in Fig. 5 were fixed at all experimental conditions and presented in Table 2. The Pd 3d spectra were fitted with a $3d_{5/2}$–$3d_{3/2}$ doublet separation of 5.25 eV and with area ratios of 3 : 2.

All these components are found in our Pd $3d_{5/2}$ spectra, but their contribution depends on reaction temperature. Pd–CO state (BE = 336.0 eV) dominates on the particle surface at $T \leq 150$ °C, but decreases at higher temperatures when the sample becomes active for CO oxidation. Cooling the sample back to RT returns the intensity of this signal to the initial level. The Pd $3d_{5/2}$ component with the

Table 2 Fitting parameters for different states of Pd 3d spectra for the bimetallic $PdAu_{low}$ sample

State	Pd $3d_{5/2}$ binding energy (eV)	FWHM (eV)	G/L
Pd_{alloy}	335.0 ± 0.1	0.7	20
$Pd_{metallic}$	335.6 ± 0.1	0.7	20
Pd–CO	336.0 ± 0.1	1.0	35
$Pd_{cluster}$	337.2 ± 0.1	1.9	45

lowest binding energy (BE = 335.1 eV), which exhibits maximum intensity in the temperature range of 230–250 °C, but is practically absent at room temperature, can be attributed to the Pd_{alloy} state. Indeed, its development with temperature correlates with the shift of the Au $4f_{7/2}$ peak to lower binding energy (Fig. 4). The lower binding energies for Pd $3d_{5/2}$ and Au $4f_{7/2}$ signals, which have been observed in a number of papers,[7,17,30] are the sign of the charge transfer from palladium to gold in the Pd–Au particles and redistribution of the Pd s-, p- and d-electrons. Metallic palladium state (BE = 335.6 eV), which is seen in the spectra within the whole temperature range, but with a higher intensity at $T \geq 200$ °C, can be presented not only as part of the bimetallic particles, but also as monometallic Pd particles not alloying with gold during the sample preparation. In both cases, the increase in intensity of this component with temperature (Fig. 5) allows us to suggest that part of the metallic palladium is located at the surface and transforms to Pd–CO state at low temperatures. It should also be noted that the intensity of the Pd $3d_{5/2}$ signal at ~336.0 eV revealed after sample heating up to 200 °C cannot be assigned to the Pd–CO state and most probably is due to oxidized Pd–O species.[35] Unfortunately, C 1s and O 1s spectra cannot be applied to prove this assignment due to overlapping of the C 1s signals from CO_{ads} and HOPG, as well as O 1s signal from Pd–O with Pd 4d region. Furthermore, oxygen adsorbed on the HOPG surface will contribute to the total O 1s spectrum.[20,38] Pd $3d_{5/2}$ signal with higher binding energies, as well as a similar one in the Au $4f_{7/2}$ spectrum (~85 eV), which were previously attributed to Pd and Au atoms decorating the HOPG surface defects,[25,37] do not change under the reaction conditions and will not be taken into account further.

Additional arguments in favor of this picture of Pd states follow from the Pd $3d_{5/2}$ spectra of monometallic Pd/HOPG samples presented in Fig. 6. The pure Pd/HOPG sample was prepared by UHV Pd deposition on the sputtered HOPG

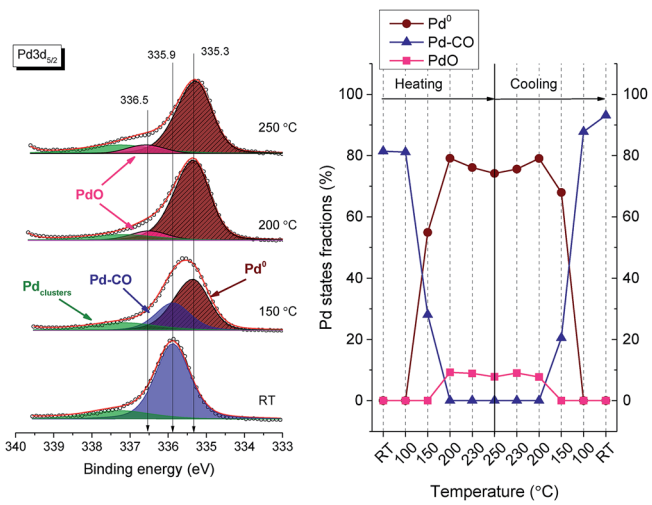

Fig. 6 Pd $3d_{5/2}$ spectra (left) and fraction of different Pd states (right) depending on the temperature taken for pure Pd/HOPG sample under the reaction mixture (spectra measured at 300 eV kinetic energy).

surface followed by heating to 300 °C (see Experimental). The mean particle size was 3.9 nm.

At room temperature the Pd/HOPG sample is characterized exclusively by a Pd–CO state (BE = 335.9 eV) which transforms to Pd metal (BE = 335.3 eV) at heating above 150 °C (Fig. 6). The absence of Pd $3d_{5/2}$ signals with lower binding energies is in line with the impossibility to produce Pd–Au alloy due to the absence of gold in this sample. Additional Pd $3d_{5/2}$ signal at 336.5 eV can be attributed to oxidized Pd–O species, with the difference in BE values for this species in pure Pd/HOPG and bimetallic Pd–Au/HOPG samples being explained by possible formation of bulk oxides in the former sample, but only surface oxide in the latter case due to dilution of palladium with gold.

To get information about the depth distribution of different Pd states, their contributions in total Pd $3d_{5/2}$ signals measured *in situ* at various temperatures were plotted as a dependence on the kinetic energies of the escaped photoelectrons (Fig. 7). Variation of kinetic energies from 300 to 600 eV increases the analysis depth in metal particles from about 6 and 9 Å (see Experimental).

At room temperature the Pd–CO contribution decreases, with a depth of analysis clearly demonstrating surface location of this species. In the active state (temperature above 200 °C) the fraction of the Pd–CO signal drops significantly indicating desorption of CO from the Pd–Au particle surface. As a consequence, this signal exhibits the lowest surface contribution (kinetic energy of 300 eV) compared with other palladium states. Furthermore, this signal increases slightly its contribution with the depth of analysis confirming that other species, but not Pd–CO, are responsible for this Pd $3d_{5/2}$ signal at these conditions. According to binding energy position, the most probable candidate is oxidized Pd–O species[28] located in subsurface layers of bimetallic Pd–Au or pure Pd particles.

In accordance with the surface location of Pd–CO species, the contribution of two other Pd species (Pd–Au alloy and Pd metal), which are quite small under reaction mixture in freshly prepared samples at RT, grows as analysis depth rises, suggesting their higher concentrations in the subsurface layers of Pd–Au particles. Desorption of CO at temperatures above 200 °C increases mostly the

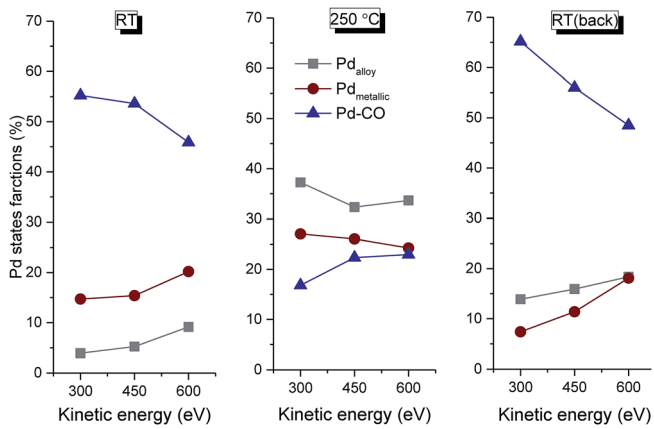

Fig. 7 Dependences of fractions of different Pd states (Pd(I)) on depth of analysis calculated for various temperatures.

contribution of alloy (about ten times) indicating incorporation of Pd atoms, which were connected earlier with CO molecules, leading to an alloy structure. As a consequence, the concentration of Pd_{alloy} is higher on the surface of metallic particles than in deeper layers. The contribution of metallic palladium does not depend on the kinetic energy of photoelectrons indicating homogeneous distribution of this species on the depth of metallic particles. Cooling back to room temperature returns in principle the depth of analysis dependencies to the initial state showing the reversibility of the temperature-induced changes in surface compositions of bimetallic Pd–Au particles. Again, the particle surface is covered by Pd atoms bonded with adsorbed CO (Pd–CO species), whereas the contribution of Pd_{alloy} species becomes smaller, increasing in the particle bulk. It should be noted that after back cooling down to RT in the CO + O_2 reaction mixture, the contribution of alloy becomes higher than that of Pd metal if compared with the initial sample. This fact confirms a significant redistribution of palladium and gold not only in the surface, but also in the bulk of bimetallic particles.

The results obtained in the current work demonstrate that the Pd–Au/HOPG model catalysts are active in the CO oxidation reaction at temperatures above 150 °C. The reaction mixture in the temperature range from RT to 150 °C causes palladium segregation on the surface of bimetallic Pd–Au particles due to CO adsorption on Pd atoms. The relatively high strength of the Pd–CO_{ads} bond makes the catalyst inactive in this temperature range. Several experimental and theoretical studies confirm the surface segregation of a more reactive alloy component – Pd in the PdAu alloyed catalysts induced by a stronger chemical bond with the adsorbate.[8,19,34,36,39] In the active state (above 150 °C) decomposition of this state due to CO desorption occurs simultaneously with PdAu alloy formation on the surface. Thus, namely the alloyed surface is responsible for the CO oxidation reaction over Pd–Au bimetallic catalysts. The reversible redistribution of the surface composition observed after cooling down to RT moves the catalysts back to the inactive state and indicates that the active site formation occurs only under reaction conditions.

The conclusion that the alloy structure provides the catalytic activity in CO oxidation is in line with the Goodman's mechanism[8,40], which suggests that gold atoms are responsible for the CO adsorption and contiguous Pd sites – for the O_2 dissociation with a further spillover of O_{ads} to Au and/or to Pd isolated sites with further CO oxidation. However, according to this mechanism, CO oxidation should occur at relatively low temperatures when weak interaction between CO and Au can provide a reasonable amount of adsorbed CO molecules. But significant segregation of Pd atoms due to formation of Pd–CO bonds can destroy the alloy structure and block the metal surface completely deactivating the catalysts. We think that such a situation was realized for the samples studied here; the initial Au/Pd ratios at the surface under reaction mixture were quite high – 0.69 and 0.28 for the $PdAu_{high}$ and $PdAu_{low}$, respectively. In this case, the mechanism of the CO oxidation reaction could be closer to that occurring on monometallic Pd samples due to a deficiency of Au atoms on the upper surface layer. In full agreement with this consideration, the activity in CO oxidation in the low temperature region was absent for both of the PdAu/HOPG catalysts, the activity being observed only at temperatures above 150 °C. The use of bimetallic model PdAu/HOPG samples with a higher Au/Pd ratio would probably lead to increasing activity within a temperature region <150 °C.

This point of view can be supported by literature data. Venezia *et al.* studied the Pd–Au/SiO_2 catalysts in the CO oxidation reaction using a plug–flow reaction.[16] They showed that the palladium-rich catalysts (10Au90Pd and 25Au75Pd) behave quite similarly in comparison with monometallic Pd catalysts. Additionally, a significant reduction of activity in CO oxidation reaction with increasing the Au fraction (50Au50Pd and 90Au10Pd) has been shown even in the low temperature range (~400 K). Probably, for the samples with low concentration of Pd, it is impossible to form contiguous Pd sites on the surface, where the O_{ads} forms, and, consequently, no CO oxidation occurs. For example, Qian and co-authors studied the CO oxidation reaction on similar Pd–Au/SiO_2 (ref. 17) catalysts and showed that for the Au–Pd alloyed particles with a high Au/Pd ratio, isolated Pd atoms dominate on the surface, while for the particles with a low Au/Pd ratio, the surface is dominated by contiguous Pd sites. They also suggested that the contiguous Pd sites are responsible for the catalyzing CO oxidation. Using a combination of analytic-potential and first-principles DFT calculations Cheng *et al.*[41] predicted that the $Au_{43}Pd_{12}$ clusters should have higher activity in the CO oxidation reaction, while the clusters with a higher or lower Au concentration should be less active. The non-monotonous dependencies between catalytic activity in CO oxidation and bimetallic Pd–Au alloy composition were suggested. In another work[19] Delannoy *et al.* used DRIFTS and ETEM to demonstrate the Pd segregation under a CO + O_2 mixture on bimetallic AuPd/TiO_2 catalysts. In this case Pd segregation correlated with a loss of activity in the CO oxidation reaction, which was explained by possible replacement of Au in low-coordinated sites by Pd atoms. Thus it looks like the optimal Au/Pd ratio, enabling the formation of contiguous Pd sites simultaneously with the Au atoms able to adsorp CO in the low temperature range, is necessary in order to achieve the highest catalytic activity of bimetallic Pd–Au/HOPG model catalyst in CO oxidation reaction.

Thus, the catalytic performance of the PdAu bimetallic catalysts in the CO oxidation reaction could strongly correlate with the initial Au/Pd ratio as well as with experimental conditions. Obviously, some more systematic studies using *in situ* techniques are necessary in order to shed light upon the nature of the active sites in bimetallic PdAu alloyed systems.

Conclusions

NAP XPS study of alloyed Pd–Au/HOPG catalysts for CO oxidation allows identification of several surface species, the concentrations of which change under the influence of reaction mixture depending on sample temperature. At low temperatures ($T \leq 150$ °C) the reaction mixture destroys the alloy structure due to surface segregation of palladium leaving gold alone in subsurface layers. The driving force of the Pd segregation is the strong adsorption of CO and the formation of Pd–CO bonds. The formation of Pd–CO surface species deactivates the alloyed particles against CO oxidation – no CO_2 formation is observed in this temperature range. Heating the sample above 150 °C results in desorption of CO molecules. Pd atoms move back into the alloy structure, and the sample becomes active in CO oxidation. Some of the Pd atoms are not incorporated into the alloy structure and exist as Pd metal, probably due to the excess of Pd in the Pd–Au samples used. Pd $3d_{5/2}$ signal with binding energy close to that of Pd–CO remaining in high temperature range (200–250 °C) probably belongs to oxidic Pd–

O species located in subsurface layers of bimetallic particles. The same species is also observed for the monometallic Pd/HOPG sample applied for the reference experiment. Cooling back down to room temperature causes the loss of catalytic activity and transformation of bimetallic particles, which again consist of almost pure gold layers covered with Pd–CO species. This result unambiguously demonstrates the importance of the application of such *in situ* techniques as NAP XPS to understand the nature of catalytically active sites.

Conflicts of interest

There are no conflicts to declare.

Acknowledgements

The authors would like to thank the Russian Science Foundation (Grant No. 14-23-00146) for the financial support of this work. NAP XPS measurements were carried out at the ISISS beamline at Helmholtz-Zentrum Berlin für Materialien und Energie.

Notes and references

1 C. W. Yi, K. Luo, T. Wei and D. W. Goodman, *J. Phys. Chem. B*, 2005, **109**, 18535–18540.
2 A. Wang, X. Y. Liu, C.-Y. Mou and T. Zhang, *J. Catal.*, 2013, **308**, 258–271.
3 V. I. Bukhtiyarov and M. G. Slin'ko, *Russ. Chem. Rev.*, 2001, **70**, 147–159.
4 L. Deng, W. Hu, H. Deng, S. Xiao and J. Tang, *J. Phys. Chem. C*, 2011, **115**, 11355–11363.
5 W. Yu, M. D. Porosoff and J. G. Chen, *Chem. Rev.*, 2012, **112**, 5780–5817.
6 M. S. Chen, D. Kumar, C. W. Yi and D. W. Goodman, *Science*, 2005, **310**, 291–293.
7 J. Xu, T. White, P. Li, C. H. He, J. G. Yu, W. K. Yuan and Y. F. Han, *J. Am. Chem. Soc.*, 2010, **132**, 10398–10406.
8 F. Gao, Y. L. Wang and D. W. Goodman, *J. Am. Chem. Soc.*, 2009, **131**, 5734–5735.
9 F. Gao, Y. Wang and D. W. Goodman, *J. Catal.*, 2009, **268**, 115–121.
10 J. C. Pritchard, Q. He, E. N. Ntainjua, M. Piccinini, J. K. Edwards, A. A. Herzing, A. F. Carley, J. A. Moulijn, C. J. Kiely and G. L. Hutchings, *Green Chem.*, 2010, **12**, 915–921.
11 S. Alayoglu, F. Tao, V. Altoe, C. Specht, Z. Zhu, F. Aksoy, D. R. Butcher, R. J. Renzas, Z. Liu and G. A. Somorjai, *Catal. Lett.*, 2011, **141**, 633–640.
12 C.-H. Liu, R.-H. Liu, Q.-J. Sun, J.-B. Chang, X. Gao, Y. Liu, S.-T. Lee, Z.-H. Kang and S.-D. Wang, *Nanoscale*, 2015, **7**, 6356–6362.
13 B. Zugic, B. L. Wang, C. Heine, D. N. Zakharov, B. A. J. Lechner, E. A. Stach, J. Biener, M. Salmeron, R. J. Madix and C. M. Friend, *Nat. Mater.*, 2017, **16**, 558–564.
14 Q. Ye, J. A. Wang, J. S. Zhao, L. N. Yan, S. Y. Cheng, T. F. Kang and H. X. Dai, *Catal. Lett.*, 2010, **138**, 56–61.
15 T. Ward, L. Delannoy, R. Hahn, S. Kendell, C. J. Purcell, C. Louis and B. D. Chandler, *ACS Catal.*, 2013, **3**, 2644–2653.

16 A. M. Venezia, L. F. Liotta, G. Pantaleo, V. La Parola, G. Deganello, A. Beck, Z. Koppány, K. Frey, D. Horváth and L. Guczi, *Appl. Catal., A*, 2003, **251**, 359–368.
17 K. Qian, L. Luo, Z. Jiang and W. Huang, *Catal. Today*, 2017, **280**, 253–258.
18 F. Gao, Y. Wang and D. W. Goodman, *J. Phys. Chem. C*, 2009, **113**, 14993–15000.
19 L. Delannoy, S. Giorgio, J. G. Mattei, C. R. Henry, N. E. Kolli, C. Methivier and C. Louis, *ChemCatChem*, 2013, **5**, 2707–2716.
20 D. V. Demidov, I. P. Prosvirin, A. M. Sorokin, T. Rocha, A. Knop-Gericke and V. I. Bukhtiyarov, *Kinet. Catal.*, 2011, **52**, 855–861.
21 A. V. Bukhtiyarov, A. V. Nartova and R. I. Kvon, *Kinet. Catal.*, 2011, **52**, 756–760.
22 A. V. Bukhtiyarov, R. I. Kvon, A. V. Nartova and V. I. Bukhtiyarov, *Russ. Chem. Bull.*, 2011, **60**, 1977–1984.
23 D. W. Goodman, *J. Catal.*, 2003, **216**, 213–222.
24 H. L. Abbott, A. Aumer, Y. Lei, C. Asokan, R. J. Meyer, M. Sterrer, S. Shaikhutdinov and H.-J. Freund, *J. Phys. Chem. C*, 2010, **114**, 17099–17104.
25 A. V. Bukhtiyarov, I. P. Prosvirin and V. I. Bukhtiyarov, *Appl. Surf. Sci.*, 2016, **367**, 214–221.
26 A. Knop-Gericke, E. Kleimenov, M. Hävecker, R. Blume, D. Teschner, S. Zafeiratos, R. Schlögl, V. I. Bukhtiyarov, V. V. Kaichev, I. P. Prosvirin, A. I. Nizovskii, H. Bluhm, A. Barinov, P. Dudin and M. Kiskinova, *Adv. Catal.*, 2009, **52**, 213–272.
27 S. Tanuma, C. J. Powell and D. R. Penn, *Surf. Interface Anal.*, 1994, **21**, 165–176.
28 http://www.uksaf.org/xpspeak41.zip.
29 J.-J. Yeh and I. Lindau, *At. Data Nucl. Data Tables*, 1985, **32**, 1–186.
30 P. A. P. Nascente, S. G. C. de Castro, R. Landers and G. G. Kleiman, *Phys. Rev. B: Condens. Matter Mater. Phys.*, 1991, **43**, 4659–4666.
31 R. W. J. Scott, C. Sivadinarayana, O. M. Wilson, Zh. Yan, D. W. Goodman and R. M. Crooks, *J. Am. Chem. Soc.*, 2005, **127**, 1380–1381.
32 A. M. Venezia, V. La Parola, G. Deganello, B. Pawelec and J. L. G. Fierro, *J. Catal.*, 2003, **215**, 317.
33 W. Jua, M. Favaro, C. Durante, L. Perini, S. Agnoli, O. Schneider, U. Stimming and G. Granozzi, *Electrochim. Acta*, 2014, **141**, 89–101.
34 R. Toyoshima, N. Hiramatsu, M. Yoshida, K. Amemiya, K. Mase, B. S. Mun and H. Kondoh, *J. Phys. Chem. C*, 2016, **120**, 416–421.
35 M. D. Strømsheim, J. Knudsen, M. H. Farstad, L. Sørvik, X. Guo, H. J. Venvik and A. Borg, *Top. Catal.*, 2017, **60**, 1439–1448.
36 M. A. Languille, E. Ehret, H. C. Lee, C. K. Jeong, R. Toyoshima, H. Kondoh, K. Mase, Y. Jugnet, J. C. Bertolini, F. J. Cadete Santos Aires and B. S. Mun, *Catal. Today*, 2016, **260**, 39–45.
37 A. V. Kalinkin, M. Y. Smirnov, A. V. Bukhtiyarov and V. I. Bukhtiyarov, *Kinet. Catal.*, 2015, **56**, 796–800.
38 G. Zhang, D. Yang and E. J. Sacher, *J. Phys. Chem. C*, 2007, **111**, 565–570.
39 H. Y. Kim and G. Henkelman, *ACS Catal.*, 2013, **3**, 2541–2546.
40 F. Gao, Y. Wang and D. W. Goodman, *J. Phys. Chem. C*, 2009, **113**, 14993–15000.
41 D. Cheng, H. Xu and A. Fortunelli, *J. Catal.*, 2014, **314**, 47–55.

